JOM, Vol. 69, No. 1, 2017
DOI: 10.1007/s11837-016-1961-7

High Temperature In Situ Compression of Thermoplastically Formed Nano-scale Metallic Glass

SANGHITA MRIDHA,[1] HARPREET SINGH ARORA,[1,2] JOSEPH LEFEBVRE,[3] SANJIT BHOWMICK,[3] and SUNDEEP MUKHERJEE[1,4]

1.—Department of Materials Science and Engineering, University of North Texas, Denton, TX 76203, USA. 2.—Department of Mechanical Engineering, School of Engineering, Shiv Nadar University, Uttar Pradesh 201314, India. 3.—Hysitron, Inc., Minneapolis, MN 55344, USA. 4.—e-mail: sundeep.mukherjee@unt.edu

The mechanical behavior of nano-scale metallic glasses was investigated by in situ compression tests in a scanning electron microscope. Platinum-based metallic glass nano-pillars were fabricated by thermoplastic forming. The nano-pillars and corresponding bulk substrate were tested in compression over the range of room temperature to glass transition. Stress–strain curves of the nano-pillars were obtained along with in situ observation of their deformation behavior. The bulk substrate as well as nano-pillars showed an increase in elastic modulus with temperature which is explained by diffusive rearrangement of atomic-scale viscoelastic units.

INTRODUCTION

Thermoplastic forming of metallic glasses has attracted much recent interest due to the ability to achieve high-strength metals in complex shapes and geometries at different length-scales.[1,2] In particular, metallic glasses formed at the nano-scale show attractive attributes in applications ranging from energy conversion[3,4] to bio-implants with favorable cell response.[5] Mechanical behavior of metallic glasses has been studied at the reduced length-scale with reports of a distinct size effect.[6,7] However, these deformation behavior studies have been mostly limited to room temperature. With the increase in temperature, atomic rearrangement and structural relaxation may significantly influence the mechanical response of amorphous metals.[8–10] Studying high-temperature effects at the nanometer length-scale may provide fundamental insights into relaxation kinetics of metallic glasses due to the small volume of material involved. Another aspect of nano-scale characterization is the synthesis route used to achieve the reduced length-scale. Uniaxial tension and compression behavior of metallic–glass nano-pillars prepared by focused-ion-beam (FIB) has been reported,[11,12] where Ga^+ ion irradiation is believed to cause significant surface damage and crystallization.[11] In contrast, thermoplastically formed nanostructures have identical thermal histories as the bulk substrate they are prepared from, without the need for secondary top–down synthesis. This allows for a direct comparison of mechanical behavior as a function of length-scale.

In this study, we investigated the high-temperature nano-mechanical behavior of thermoplastically formed platinum-based metallic glass (MG). Thermoplastic forming was used to synthesize metallic glass nano-pillars of a Pt-based amorphous alloy, $Pt_{57.5}Cu_{14.7}Ni_{5.3}P_{22.5}$. Nano-pillars and the corresponding bulk substrate were tested in compression over a wide temperature range. The bulk substrate as well as nano-pillars showed an increase in elastic modulus with temperature. Engineering stress–strain response was obtained for the nano-pillars concurrent with in situ observation of their deformation and failure.

EXPERIMENTAL

A fully amorphous alloy with nominal composition, $Pt_{57.5}Cu_{14.7}Ni_{5.3}P_{22.5}$, was prepared in a vacuum-sealed silica tube by melting high-purity constituents.[1,2] Amorphous cylinders were obtained by water quenching the molten samples after appropriate B_2O_3 fluxing. The as-cast alloy was thermoplastically processed in the supercooled liquid region above the glass transition temperature. X-ray diffraction (XRD) and transmission electron

(Published online May 26, 2016)

microscopy (TEM) were used to characterize the structure of the alloy after processing. The glass transition temperature (T_g) and crystallization temperature (T_x) of the processed alloy were obtained using differential scanning calorimetry (DSC) at a heating rate of 20°C/min. XRD was performed using a Rigaku III Ultima x-ray diffractometer with Cu-K_α radiation of wavelength 1.54° A. TEM specimen was prepared for the thermoplastically processed alloy by conventional sample preparation technique. Nano-indentation was done using a Hysitron Triboindenter (Hysitron, Minneapolis, MN, USA) for a wide temperature range using a high-temperature diamond Berkovich tip. The indentation was performed at a load of 10,000 μN with a loading time of 5 s, a hold time of 2 s and an unloading time of 5 s. Ten indents were performed at each temperature. The distance between two neighboring indents was maintained larger than 10 μm to avoid overlap of their plastic zones. A constant flow of inert Ar + H_2 mixture was maintained to prevent oxidation of the sample and the diamond tip.

To obtain nano-pillars, the amorphous alloy was thermoplastically processed in the supercooled liquid region above its glass transition temperature using commercially available alumina nano-molds.[1,2] The nano-pillars had an average diameter of 200 nm. A few nano-pillars were selected and an area of 4 μm diameter around the nano-pillar was removed using focused-ion-beam. In situ quasi-static compression tests were performed on the nano-pillars at room temperature and elevated temperature using a PI 85 scanning electron microscope (SEM) PicoIndenter (Hysitron) with a 2-μm flat punch diamond probe inside a SEM (Versa 3D FIBSEM, FEI). In situ heating of the sample was achieved using a resistive micro-electro-mechanical system (MEMS) heater. The heating element is composed of an integrated thin film of platinum on quartz. High-temperature conductive epoxy (EPO TEC) was used to mount the sample on the heating stage, with the MEMS heater underneath. Compression tests on the nano-pillars were performed at temperatures of 25°C, 160°C, and 180°C at a strain rate of 2×10^{-3} s^{-1}. Three measurements were done at each temperature.

RESULTS AND DISCUSSION

The DSC curve for a thermoplastically processed metallic glass sample is depicted in Fig. 1a. The glass transition temperature (T_g) and crystallization temperature (T_x) were 225°C and 290°C, respectively. XRD showed the fully amorphous structure for the metallic glass (Fig. 1b). High-resolution transmission electron microscope (HRTEM) image for the Pt-based MG along with the selected area electron diffraction (SAED) pattern can be seen in Fig. 1c. The diffused halo in the diffraction pattern confirms the amorphous structure.

The load–displacement curves obtained from nano-indentation of the processed bulk alloy as a function of temperature are shown in Fig. 2a. The average and standard deviation of ten measurements at each temperature are shown in the figure. The hardness and reduced modulus were obtained from load displacement curves using Oliver and Pharr method[13] (Fig. 2b). The hardness (H) was evaluated using Eq. 1, and the reduced modulus (E_r) was evaluated from stiffness (S) using Eqs. 2 and 3. In Eqs. 1–3, P_{max} is the maximum load, A is contact area, E and E_i (=1141 GPa) are the Young's modulus of the sample and diamond indenter respectively; ν and ν_i (=0.07) are the Poisson's ratio of the sample and diamond indenter, respectively; and β is a constant (value of 1.05 used for the Berkovich tip).

$$H = \frac{P_{max}}{A} \tag{1}$$

$$S = \frac{dP}{dh} = \beta \frac{2}{\sqrt{\pi}} E_r \sqrt{A} \tag{2}$$

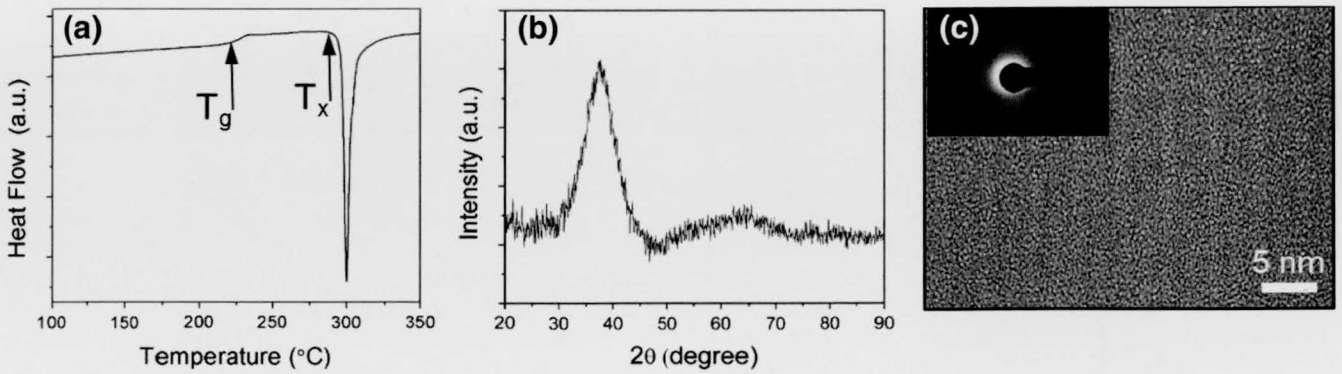

Fig. 1. (a) Differential scanning calorimetry curve for $Pt_{57.5}Cu_{14.7}Ni_{5.3}P_{22.5}$ metallic glass (Pt MG); (b) x-ray diffraction for Pt MG substrate; (c) High-resolution transmission electron microscopy image for the Pt MG substrate after thermoplastic forming. Inset in (c) shows the selected area electron diffraction pattern with amorphous halo.

$$\frac{1}{E_r} = \frac{1-\nu^2}{E} + \frac{1-\nu_i^2}{E_i} \quad (3)$$

High-temperature measurements using nano-indentation were done up to 180°C. The discrete displacement jumps in the loading curves indicate shear banding in metallic glasses.[14] With an increase in temperature, serration frequency decreases along with an increase in serration step length. This is attributed to the transition from inhomogeneous deformation at low temperatures to homogeneous deformation at high temperatures.[14,15] Variation in

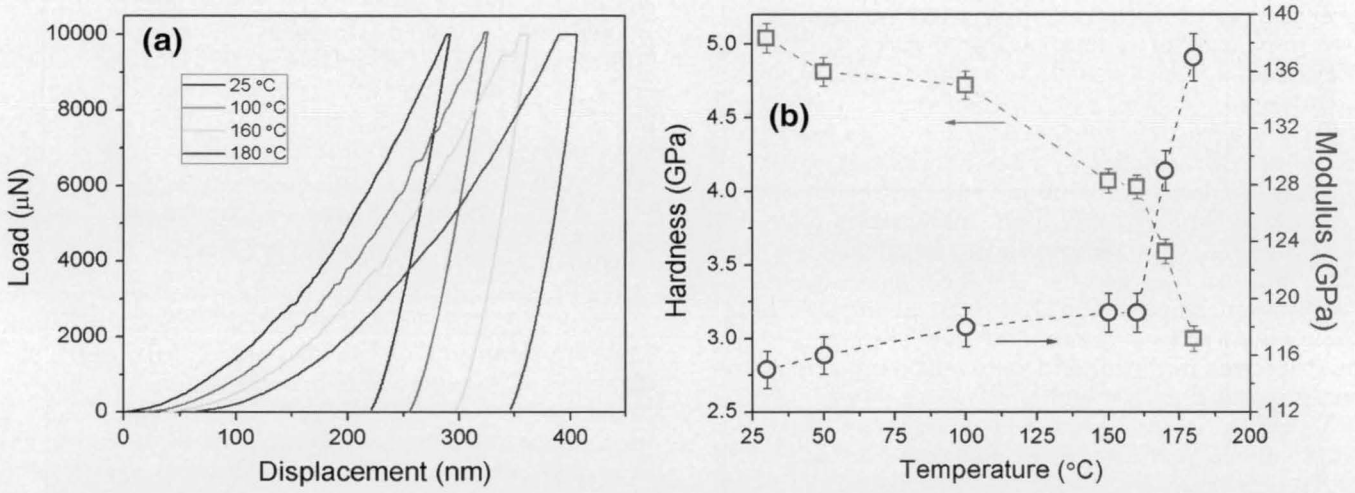

Fig. 2. (a) Load–displacement curves obtained from nano-indentation over a wide temperature range for the Pt MG substrate; (b) variation in elastic modulus and hardness for Pt MG substrate as a function of temperature. The average and standard deviations of ten measurements at each temperature are shown.

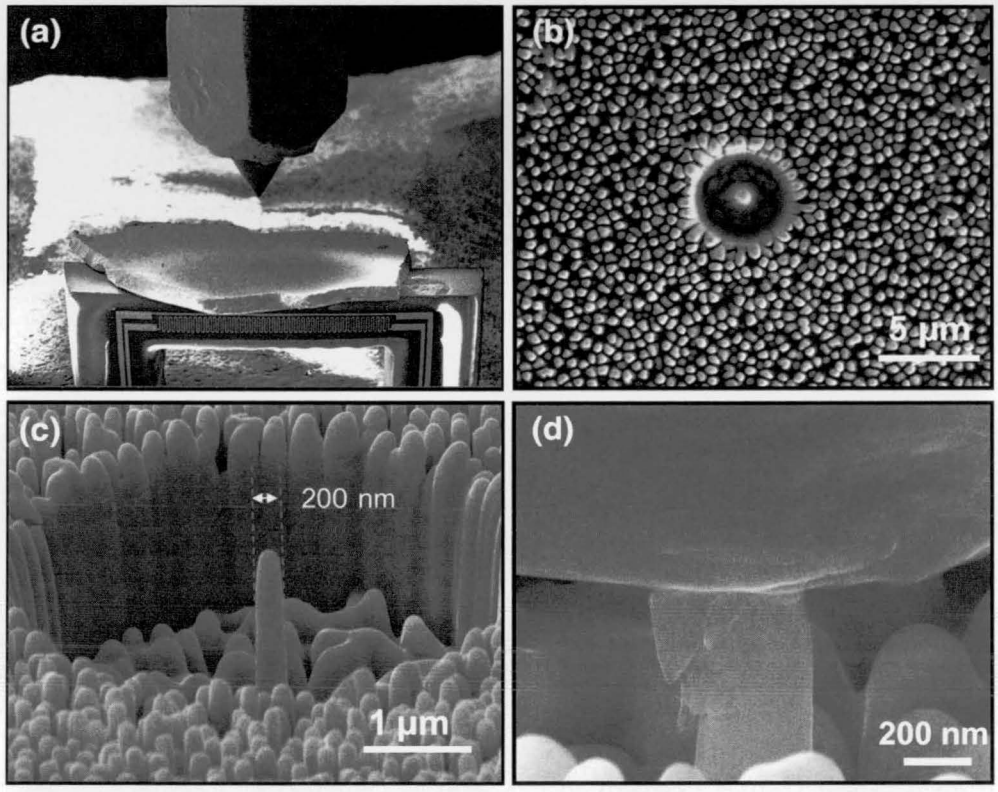

Fig. 3. (a) SEM image of picoindenter setup used in the current study showing the heating stage and the indenter; (b) top view of the Pt MG nano-pillar selected for in situ compression testing; (c) SEM image showing slight taper in the Pt MG nano-pillar; (d) SEM image at the end of compression testing showing catastrophic shearing.

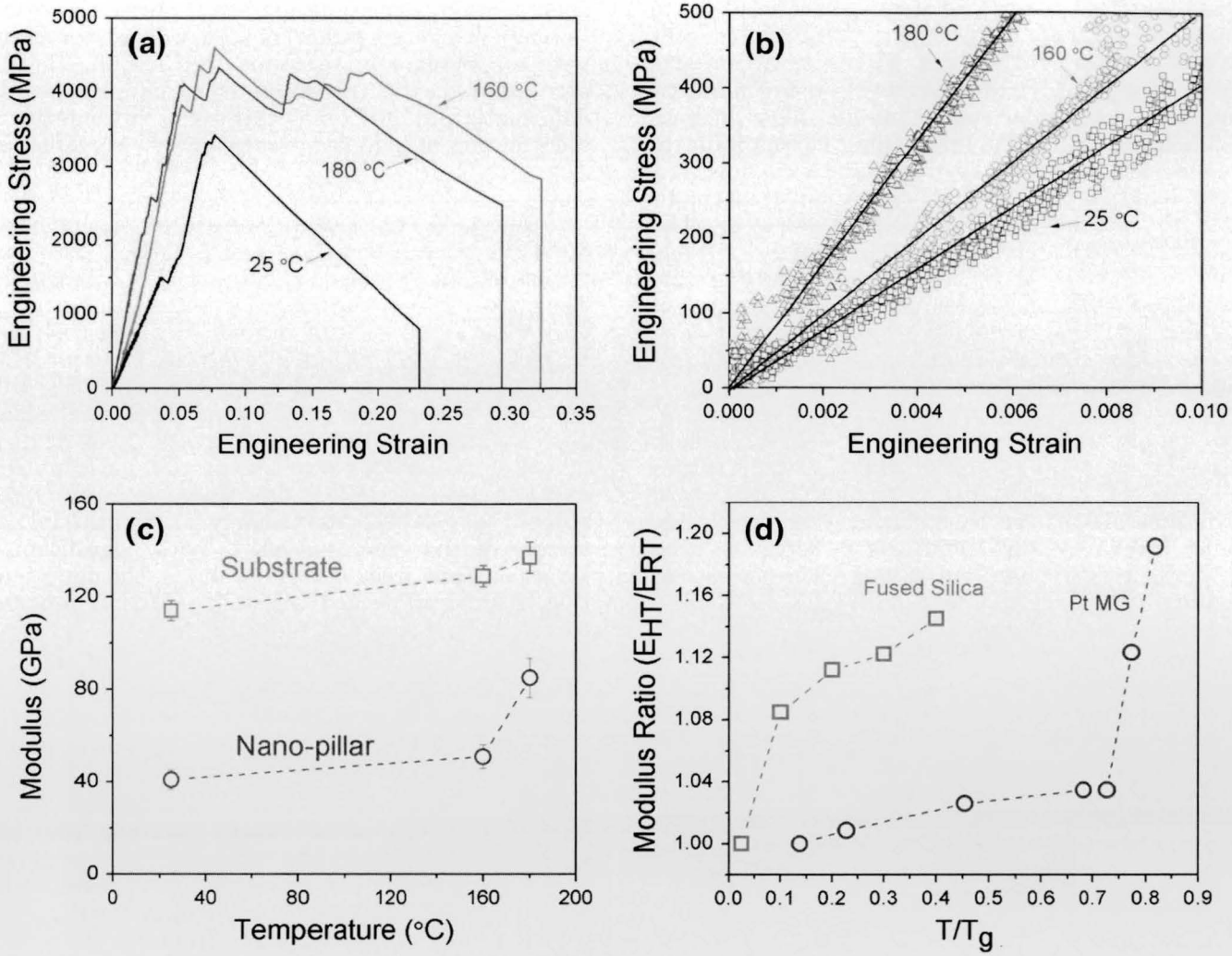

Fig. 4. (a) Engineering stress–strain curves of Pt MG nano-pillars at different temperatures; (b) zoomed-in view of the initial portion of the stress–strain curve; (c) comparison of modulus variation with temperature for the Pt MG substrate and Pt MG nano-pillar. For the substrate, the average and standard deviation are plotted based on ten measurements, while three measurements were done at each temperature for the nano-pillars; (d) variation of the modulus ratio, high-temperature elastic modulus (E_{HT}) to room temperature modulus (E_{RT}), as a function of temperature for the Pt MG substrate and fused silica,[22] normalized by the respective glass transition temperature.

the modulus, calculated from the unloading curve as a function of temperature, is shown in Fig. 2b. There was a gradual increase in the reduced modulus at low temperatures followed by sharp increase close to the peak measurement temperature of 180°C. In contrast, hardness continuously decreased over the entire temperature range (Fig. 2b) from a value of 5 GPa at room temperature to below 3 GPa at 180°C. The decrease in hardness may be attributed to the change in the deformation mechanism from heterogeneous to homogeneous deformation. A decrease in hardness with the change in deformation mechanism[16] and the transition temperature lying between 0.7 and 1.1 T_g have been reported earlier.[14,16–18] Heterogeneous deformation is characterized by linear elastic flow followed by shear localization. Homogeneous deformation could occur by non-Newtonian or Newtonian flow depending on the strain rate.[16]

Figure 3a shows the SEM image of the pico-indenter setup used in the current study, including the heating stage, MEMS heater, and the indenter. Figure 3b and c shows one of the nano-pillars used for the compression test, with the surrounding area cleared using the focused-ion-beam. The nano-pillar has a diameter of ~200 nm and height of ~1.5 μm. The pillars have some degree of taper which was estimated to be in the range of 3°–5° using ImageJ software. The nano-pillar at the end of compression test indicates that failure occurred by catastrophic shearing (Fig. 3d). Shear bands are clearly observed on the deformed nano-pillar surface. Representative engineering stress–strain curves for the nano-pillars at each of the three temperatures are shown in Fig. 4a. The stress–strain curves for the nano-pillars reveal serrations, which denote shear banding during sub-T_g

compression. Taper in the nano-pillars is likely to affect the stress–strain curve.[19,20] Stress concentration at the top of the pillar may result in early initiation of shear bands during the compression test. For a taper of ~5°, the yield strength is overestimated by approximately 50% compared to the corresponding taper-free pillars.[19] However, shear band instabilities in tapered pillars complicates the estimation of the elastic modulus. The instabilities are enhanced at the reduced length-scale due to the high elastic energy stored in nano-pillars.[21] Figure 4b shows the zoomed-in view of the initial portion of the stress–strain curve, which was used to calculate their elastic modulus. Comparison of elastic modulus as a function of temperature for the bulk substrate and the corresponding nano-pillar (Fig. 4c) demonstrates that, in both cases, the modulus increases with the temperature rise. For the substrate, the average and standard deviations are plotted based on ten measurements, while three measurements were done at each temperature for the nano-pillars. The measured modulus values for the nano-pillars are smaller by almost a factor of three compared to the corresponding substrate. This difference may be partly explained by the taper in the nano-pillars as well as misalignment between the nano-pillars and the compression axis.[19] The variation of the modulus ratio, the high-temperature modulus (E_{HT}) to room-temperature modulus (E_{RT}), as a function of temperature normalized by the glass transition temperature is shown in Fig. 4d. The Pt-based MG modulus ratio increased nearly 1.2 times at the peak temperature of 180°C compared to room temperature. A similar behavior vis-à-vis the increase in the elastic modulus with temperature has been reported for silicate glasses.[22] An initial sharp rise in the modulus of fused silica with temperature followed by saturation may be explained by densification resulting from compaction of its open three-dimensional coordinated structure. However, in the case of the metallic glass, the change is very gradual with the initial temperature rise followed by a sharp increase close to the glass transition.

The observed temperature-dependence of the elastic modulus for the metallic glass may be explained by the core–shell geometry of its intrinsic viscoelastic units which consist of soft free volume zones and a surrounding elastic envelop.[23] For a metallic glass deformed at room temperature, high activation energy for atomic rearrangement causes flow incompatibility between the deforming zone and the surrounding un-deformed material and results in shear flow. At high temperature, metallic glasses show significant relaxation. During the relaxation process, the rate of free volume annihilation follows an exponential relationship with temperature and can be expressed by Eq. 4 below:[8]

$$\frac{dC_f(t,T)}{dt} = -C_0 \exp\left(-\frac{E_f}{RT}\right) C_f(C_f - C_{fe}) \quad (4)$$

where $C_f(t,T) = \exp\left(-\frac{1}{\vartheta_f}\right)$ is the flow defect concentration and ϑ_f is the non-equilibrium amount of free volume on the order of 10^{-3}/atomic volume;[24] $C_{fe} = \exp(-\frac{1}{\vartheta_{fe}})$ is the equilibrium flow defect concentration, E_f is the activation energy on the order of 100 kJ/mole,[25] and C_0 is a variable parameter on the order of 10^{23} s^{-1}.[25] The localized stress-field associated with compression accompanied by diffusive rearrangement of atomic-scale viscoelastic units at high temperature results in the annihilation of free volume and densification. Therefore, shear flow at low temperature compared to relaxation-induced densification at elevated temperature explains the sharp increase in the modulus for metallic glasses. Molecular dynamic simulation reveals that surface atoms carry most of the initial strain during deformation.[12] With significantly larger surface areas per unit volume, the densification in nano-pillars is likely to be higher compared to the bulk substrate. This explains the greater degree of modulus increase for the nano-pillars compared to the corresponding bulk.

CONCLUSION

In summary, the high-temperature mechanical behavior of thermoplastically formed metallic glass nano-pillars was investigated. Pt-based metallic glass nano-pillars and the corresponding bulk substrate were tested in compression from room temperature up to 180°C. At both length-scales, the metallic glass demonstrated an increase in the modulus with temperature, which is explained by a diffusive rearrangement of atomic-scale viscoelastic units. The degree of stiffness increase was greater for the nano-pillars compared to the bulk.

REFERENCES

1. J. Schroers, *Adv. Mater.* 22, 1566 (2010).
2. G. Kumar, H.X. Tang, and J. Schroers, *Nature* 457, 868 (2009).
3. M. Carmo, R.C. Sekol, S. Ding, G. Kumar, J. Schroers, and A.D. Taylor, *ACS Nano* 5, 2979 (2011).
4. S. Mukherjee, R.C. Sekol, M. Carmo, E.I. Altman, A.D. Taylor, and J. Schroers, *Adv. Funct. Mater.* 23, 2708 (2013).
5. J. Padmanabhan, E.R. Kinser, M.A. Stalter, C. Duncan-Lewis, J.L. Balestrini, A.J. Sawyer, J. Schroers, and T.R. Kyriakides, *ACS Nano* 8, 4366 (2014).
6. D. Jang and J.R. Greer, *Nat. Mater.* 9, 215 (2014).
7. L. Tian, Y. Cheng, Z. Shan, J. Li, C. Wang, X. Han, J. Sun, and E. Ma, *Nat. Commun.* 3, 609 (2012).
8. P. Murali and U. Ramamurty, *Acta Mater.* 53, 1467 (2005).
9. A. Slipenyuk and J. Eckert, *Scr. Mater.* 50, 39 (2004).
10. B.B. Medeiros, M.M. Medeiros, J. Fornell, J. Sort, M.D. Baró, and A.M. Jorge, *J. Non Cryst. Solids* 2, 103 (2015).
11. D. Magagnosc, R. Ehrbar, G. Kumar, M. He, J. Schroers, and D. Gianola, *Sci. Rep.* 3, 1 (2013).
12. D. Chen, D. Jang, K. Guan, Q. An, W. Goddard III, and J. Greer, *Nano Lett.* 13, 4462 (2013).
13. W.C. Oliver and G.M. Pharr, *J. Mater. Res.* 19, 3 (2004).

14. C.A. Schuh, A.C. Lund, and T. Nieh, *Acta Mater.* 52, 5879 (2004).
15. H.S. Arora, A.V. Aditya, and S. Mukherjee, *J. Appl. Phys.* 117, 014902 (2015).
16. J. Lu, G. Ravichandran, and W.L. Johnson, *Acta Mater.* 51, 3429 (2003).
17. P. Wesseling, T. Nieh, W. Wang, and J. Lewandowski, *Scr. Mater.* 51, 151 (2004).
18. A. Argon and L.T. Shi, *Acta Metall.* 31, 499 (2004).
19. B. Schuster, Q. Wei, T. Hufnagel, and K. Ramesh, *Acta Mater.* 56, 5091 (2008).
20. O.V. Kuzmin, Y.T. Pei, C.Q. Chen, and J.T.M. De Hosson, *Acta Mater.* 60, 889 (2012).
21. Z. Wu, Y. Zhang, M.H. Jhon, H. Gao, and D.J. Srolovitz, *Nano Lett.* 12, 910 (2012).
22. B.D. Beake and J.F. Smith, *Philos. Magn. A* 82, 2179 (2002).
23. J. Ye, J. Lu, C. Liu, Q. Wang, and Y. Yang, *Nat. Mater.* 9, 619 (2010).
24. A. Slipenyuk and J. Eckert, *Scr. Mater.* 50, 39 (2004).
25. A. Van den Beukel and J. Sietsma, *Acta Metall. Mater.* 38, 383 (1990).